Bβ Glu397 and Bβ Asp398 but Not Bβ Asp432 Are Required for "B:b" Interactions[†,‡]

Michael S. Kostelansky,[⊥] Bettina Bolliger-Stucki,[||] Laurie Betts,[§] Oleg V. Gorkun,[||] and Susan T. Lord*[,||,⊥]

Department of Chemistry, Department of Pharmacology, and Department of Pathology and Laboratory Medicine, University of North Carolina, Chapel Hill, North Carolina 27599

Received November 8, 2003; Revised Manuscript Received December 20, 2003

ABSTRACT: We synthesized three fibrinogen variants, Bβ E397A, Bβ D398A, and Bβ D432A, with substitutions at positions identified in crystallographic studies as critical for binding the "B" peptide, Gly-His-Arg-Pro-amide (GHRPam), to the "b" polymerization site. We examined thrombin- and batroxobin-catalyzed polymerization by turbidity measurements and found that Bβ E397A and Bβ D398A were impaired while Bβ D432A was normal. Changes in polymerization as a function of calcium were similar for variant and normal fibrinogens. We determined crystal structures of fragment D from the variant Bβ D398A in the absence and presence of GHRPam. In the absence of peptide, the structure showed that the alanine substitution altered only specific local interactions, as alignment of the variant structure with the analogous normal structure resulted in an RMSD of 0.53 Å over all atoms. The structure also showed reduced occupancy of the β2 calcium-binding site that includes the side chain carbonyl of Bβ D398, suggesting that calcium was not bound at this site in our polymerization studies. In the presence of peptide, the structure showed that GHRPam was not bound in the "b" site and the conformational changes associated with peptide binding to normal fragment D did not occur. This structure also showed GHRPam bound in the "a" polymerization site, although in two different conformations. Calcium binding was associated with only one of these conformations, suggesting that calcium binding to the γ2-site and an alternative peptide conformation were induced by crystal packing. We conclude that Bβ E397 and Bβ D398 are essential for the "B:b" interaction, while Bβ D432 is not.

Fibrinogen is a 340 kDa dimeric glycoprotein composed of two copies of three nonidentical polypeptide chains, Aα, Bβ, and γ. The six chains fold to form an elongated trinodular molecule in which two terminal nodules designated D flank a central nodule, E (*1*, *2*). The amino termini of all six chains fold together into the central E nodule. Two coiled-coil connectors, each composed of the three polypeptide chains, extend in opposite directions from the center to link the D and E nodules (*3*). The carboxyl termini of the Bβ- and γ-chains fold independently into two globular modules in the D nodule, while the carboxyl termini of the Aα-chains either fold back to associate noncovalently with the central E nodule or extend freely in solution (*4*).

X-ray crystallography studies of the D nodule fragment showed that the β- and γ-chains share not only sequence homology but also significant structural similarity (*5*). Four calcium-binding sites were identified in the crystal structures, two sites in the γ-module and two in the β-module (*5*−*9*). We have designated these sites as γ1, γ2, β1, and β2, where γ1 and β1 are analogous sites but γ2 and β2 are not. The biochemically characterized, high-affinity calcium-binding site, designated γ1, is composed of the side chains of residues γ Asp318 and γ Asp320, and the backbone carbonyls of γ Phe322 and γ Gly324. The γ2-site, comprised of the side chains of γ Asp294 and γ Asp301 and backbone carbonyls of γ Gly296 and γ Asp298, is apparent in crystal structures only when the peptide GHRPam is bound to the γ-chain polymerization site (*8*). The β1-site, analogous to the γ1-site, is formed by the side chains of Bβ Asp381 and Bβ Asp383 and the backbone carbonyl of Bβ Trp385. The β2-site, which is not analogous to the γ2-site, includes the side chains of Bβ Asp261, Bβ Asp398, and γ Glu132 and the backbone carbonyl oxygen of Bβ Gly263. The β2-site serves as an anchor linking the β-module and the coiled-coil connector (*8*, *9*). This anchor carries out a significant biological function during polymerization (*9*).

The conversion of soluble fibrinogen to an insoluble fibrin clot begins when thrombin cleaves fibrinopeptides A and B (FpA and FpB)[1] from the amino termini of the Aα- and Bβ-chains of fibrinogen, respectively. The removal of FpA

[†] This work was supported by National Institutes of Health Grant HL 31048 (S.T.L.).

[‡] The atomic coordinates have been deposited in the Protein Data Bank (www.rcsb.org) under the access codes 1RE4 (rfD-Bβ D398A) and 1RE3 (rfD-Bβ D398A+GH).

* Corresponding Author: Susan T. Lord, Ph.D, University of North Carolina at Chapel Hill, Department of Pathology and Laboratory Medicine, CB #7525, Brinkhous-Bullitt Building room 822, Chapel Hill, NC 27599-7525. Phone: (919) 966−3548. Fax: (919) 966-6718. E-mail: stl@med.unc.edu.

[⊥] Department of Chemistry.

[||] Department of Pathology and Laboratory Medicine.

[§] Department of Pharmacology.

[1] Abbreviations: rfD, recombinant fibrinogen fragment D; rfD-BOTH, recombinant fibrinogen fragment D with GPRPam and GHRPam bound; rfD-Bβ D398A, fragment D of Bβ D398A fibrinogen; rfD-Bβ D398A+GH, fragment D of Bβ D398A fibrinogen with GHRPam bound; GPRPam, Gly-Pro-Arg-Pro-amide; GHRPam, Gly-His-Arg-Pro-amide; FpA, fibrinopeptide A; FpB, fibrinopeptide B; HEPES, *N*-(hydroxyethyl)piperazine-*N*′(2-ethanesulfonic acid); NAG, *N*-acetylgalactosamine; FUC, fucose; EDTA, ethylenediaminetetraacetic acid.

10.1021/bi035996f CCC: $27.50 © 2004 American Chemical Society
Published on Web 02/10/2004

exposes polymerization site "A" (Gly-Pro-Arg-Val sequence), while FpB removal uncovers polymerization site "B" (Gly-His-Arg-Pro sequence) (*10*, *11*). The newly formed "A" and "B" polymerization sites of one fibrin molecule interact with inherent polymerization sites "a" and "b" located in the γ- and β-modules, respectively, of another fibrin molecule. Fibrin monomers associate with one another through "A" and "a" interactions ("A:a") to form half-staggered, double-stranded protofibrils that grow to a critical length prior to their aggregation into thick, branching fibrin fibers (*12*, *13*). FpB release occurs predominantly during protofibril formation, suggesting that "B:b" interactions enhance the lateral aggregation of protofibrils (*12*, *14*). Nevertheless, the specific role of the "B:b" interaction remains unclear. Indeed, analysis of polymerization initiated with thrombin-like enzymes that cleave only FpA, such as batroxobin, suggested that "A:a" interactions alone are enough to form fibrin clots (*12*, *15*). In support of this idea, analysis of clot formation in whole blood showed only a fraction of FpB was missing from a fibrin clot (*16*). Conversely, recent analysis of variant fibrinogens with weakened "A:a" interactions suggests that "B:b" interactions can support protofibril formation (*17*).

The enigmatic role of the "B:b" interaction has hindered researchers in their quest to fully characterize the steps of fibrinogen polymerization. Early crystallography studies defined the "A:a" interaction by showing a peptide mimic of the "A" polymerization site (GPRPam) bound to a pocket in the C-terminal region of the γ-module (*5*, *18*). Shortly thereafter the "B:b" interaction was seen in similar models based on crystals grown with a peptide mimic of the "B" polymerization site (GHRPam) (*7*, *8*). The resulting structures showed the peptide bound in a pocket located in the carboxyl terminal region of the β-module to form a "B:b" interaction analogous to "A:a". Substantive conformational changes within the "b" polymerization site were seen with bound GHRPam. Specifically, residues BβGlu397 and BβAsp398 flipped 180° from their original positions to interact with the bound peptide in the "b" polymerization site (*8*). Further, binding GHRPam to the "b" site also eliminated the nearby β2 calcium-binding site (*9*). Although the crystallographic data provide clear snapshots of the "B" peptide bound in the "b" site, the true dynamics of "B:b" interactions in fibrin polymerization remain hidden in conflicting biochemical data. The "A:a" and "B:b" interactions were first studied in equilibrium dialysis experiments with peptide mimics of the "A" (GPRP) and "B" (GHRP) sites to measure binding affinities (*10*, *19*). These studies showed that "B:b" interactions were substantially weaker than "A:a" interactions. Further studies showed that GPRP could inhibit polymerization while GHRP could not, indicating that the "A:a" interaction was essential while the "B:b" interaction was not. Consistent with these observations, many dysfunctional fibrinogens with mutations in the "a" site have been reported (*20*), while no dysfunctional fibrinogens with "b" site modifications have been discovered. A potential role for the "B:b" interactions was seen in more recent studies with variant fibrinogens that had weakened "A:a" interactions. Polymerization of these variants was inhibited by GHRPam, suggesting that "B:b" interactions do contribute to protofibril formation (*17*). A multitude of studies have suggested that "B:b" is involved in the lateral aggregation of protofibrils (*12*−*15*). For example, when thrombin was added to batroxobin-generated fibrin, the fibers were thicker than with batroxobin alone (*21*). We initiated the current studies to better define the role of "B:b" interactions.

This manuscript describes the first account of experiments that combine the techniques of protein engineering and X-ray crystallography to synthesize and examine functional mutations in fibrinogen. To investigate the role of the "b" polymerization site in fibrin clot formation, we synthesized three variant fibrinogens with single amino acid substitutions at residues shown to interact with the peptide GHRPam. The "b" site residues BβGlu397, BβAsp398, and BβAsp432 were each replaced with alanine. One residue, BβAsp398, also coordinates the β2 calcium-binding site, though only when GHRP is not bound in the "b" polymerization site. We expected replacement of BβAsp398 with alanine would disrupt both calcium and GHRP binding, while the other single alanine replacements would disrupt only GHRP binding. We used biochemical assays to determine the effects of these changes on polymerization. To assess the affects of our mutations on fibrinogen structure, we solved X-ray crystal structures of recombinant fragment D from the BβD398A variant (rfD-BβD398A) with and without the peptide GHRPam. When taken together, our data indicate that residues BβGlu397 and BβAsp398 are essential to "B:b" interactions, while residue BβAsp432 is not.

MATERIALS AND METHODS

Reagents. All chemicals used in this study were analytical grade and were purchased from Sigma (St. Louis, MO), unless otherwise noted. Human thrombin was obtained from Enzyme Research Laboratories, Inc. (South Bend, IN). Batroxobin (*Batroxobin moojeni*) was purchased from Center-Chem (Stamford, CT). The peptide GHRPam was synthesized by the Protein Chemistry Lab of the University of North Carolina (Chapel Hill, NC). Culture medium with normal recombinant fibrinogen was obtained from the National Cell Culture Center (Minneapolis, MN). Cyanogen bromide activated Sepharose 4B resin was purchased from Amersham Biosciences (Piscataway, NJ). Monoclonal antibody IF-1 was purchased from Iatron Corp. (Tokyo, Japan).

Construction of Mutant Expression Vectors. The previously described Bβ-chain expression vector, pMLB-Bβ (*22*), was altered by site-directed mutagenesis using the techniques and materials as described (*23*) with slight modifications. Transfections of competent cells were performed by heat shock, and the plasmid DNA was purified from overnight bacteria cultures using an alkaline lysis protocol.

Three mutant vectors were constructed using primers to change BβGlu397 to Ala, BβAsp398 to Ala and BβAsp432 to Ala. The primer for BβGlu397 to Ala was 5′CCCAGAAAACAGTGTTCTAAAGC∗AGACGGTGGTGGATGG3′, for BβAsp398 to Ala 5′CCCAGAAAACAGTGTTCTAAAGAAG∗CCGGTGGTGGATGG3′, and BβAsp432 to Ala 5′GCATGGCACAGC∗TGATGGTGTAGTATGG3′, where the ∗ indicates the base substitution. To facilitate the screening of potential mutant clones, each primer also changed a restriction site: the vectors encoding BβAla397 and BβAla398 lost a BbsI site and the vector encoding BβAla432 introduced an additional PvuII site. Clones with the appropriate restriction site patterns were selected, and

the complete Bβ-chain cDNA was sequenced to confirm the modified codon and ensure that no unanticipated changes were incorporated (data not shown). The new plasmids were named pMLP BβE397A, pMLP BβD398A, and pMLP BβD432A. DNAs for Chinese hamster ovary (CHO) cell transfection were prepared with the Qiagen Plasmid Kit (Qiagen, Valencia, CA).

Recombinant Fibrinogen Expression and Purification. Recombinant fibrinogens were expressed essentially as described (*22*). Briefly, each plasmid, pMLP BβE397A, pMLP BβD398A, and pMLP BβD432A, was cotransfected with pMSV His into cells previously transfected with plasmids pMLP Aα, pMLP γ, and pRSV-neo as described (*24*). Clones were selected on the basis of neomycin and histidinol resistance, and the culture medium was screened for fibrinogen by enzyme-linked immunosorbent assay (ELISA). Cell lines producing high levels of fibrinogen were used for large-scale cultures grown in roller bottles supplemented with micro-carrier beads (*22*). Serum-free medium containing recombinant fibrinogen was harvested twice a week from several roller bottles and pooled, and phenylmethylsulfonyl fluoride was added to 0.15 mM. The medium was stored at −20 °C until purification.

The normal and variant proteins were purified as described (*25*). In brief, the medium was thawed at 37 °C, fibrinogen was precipitated with ammonium sulfate, and the precipitate was dissolved in a buffer containing 10 mM $CaCl_2$. The sample was separated on Sepharose 4B coupled with the calcium-dependent monoclonal antibody IF-1, and fibrinogen was eluted with 5 mM EDTA. The purified protein was dialyzed at 4 °C first against 20 mM HEPES, pH 7.4, and 150 mM NaCl (HBS buffer) containing 1 mM calcium chloride and, subsequently, against HBS buffer at 4 °C. The fibrinogen concentration was determined from A_{280} using the extinction coefficient ϵ_{280} of 1.506 for a 1 mg/mL solution (*26*). Purified fibrinogen was characterized on a 10% gel by SDS−PAGE. The proteins were stored at −70 °C.

Kinetics of Fibrinopeptide Release. Fibrinopeptide release was monitored essentially as described (*22*, *27*). Fibrinogen was diluted in HBS to 0.1 mg/mL; human α-thrombin or batroxobin was added to a final concentration of 0.005 U/mL. The reactions were performed at ambient temperature and were stopped at designated time points by boiling for 15 min. To measure the total fibrinopeptide A and B released, fibrinogen was incubated with 10 U/mL thrombin or batroxobin for 240 min. Samples were centrifuged (10 min; Microfuge, Fisher), and the supernatants were immediately analyzed by reversed-phase HPLC, using the Shimadzu HPLC system (Shimadzu, Columbia, MD) with a Discovery C18 column with dimensions 25 cm × 4.6 mm, 5 μm (Supelco, Bellefonte, PA). The column was equilibrated with buffer A (25 mM NaH_2PO_4/Na_2HPO_4, pH 6.0), and 200 μL of each sample was loaded onto the column with an autosampler. The peptides were eluted with a linear gradient from 15% to 36% buffer B (25 mM NaH_2PO_4/Na_2HPO_4, pH 6.0, with 50% acetonitrile). The elution of peptides was monitored by absorbance at 210 nm. Peak areas were determined using the accompanying software Class 5.0 VP (Shimadzu). Fibrinopeptide release curves were constructed from two experiments plotting the percent released, assuming the total FpA release from normal fibrinogen was 100%.

Thrombin-Catalyzed Polymerization. Thrombin-induced polymerization was monitored at 350 nm in a SpectraMax-340PC Microplate reader at room temperature (Molecular Devices, Sunnyvale, CA), essentially as described (*28*). At least three separate experiments were performed for each polymerization condition. The reactions were performed at ambient temperature in 20 mM HBS with 10 mM, 1mM, or no added $CaCl_2$. The Cl^- ion concentration was kept constant at 150 mM by adjusting the concentration of NaCl. Each reaction well contained 90 μL of 0.22 mg/mL fibrinogen. Polymerization was initiated by adding 10 μL of 1 U/mL α-thrombin with a multichannel pipet such that all reactions began simultaneously. Immediately after addition of the enzyme, the samples were mixed for 5 s with the automix feature of the plate reader. Turbidity was monitored every 24 s for 3 h.

Batroxobin-Catalyzed Polymerization. Batroxobin-induced polymerization was monitored at 350 nm for 40 min using a BioSpec-1601 spectrophotometer (Shimadzu), essentially as described (*25*). Polymerization was performed in a quartz microcuvette, the reaction being initiated by the addition of 10 μL of 1 U/mL batroxobin to 90 μL of 0.11 mg/mL fibrinogen. The reactions were performed at ambient temperature in 20 mM HBS with 1 mM or 1 μM $CaCl_2$. The Cl^- ion concentration was kept constant at 150 mM by adjusting the concentration of NaCl.

Analysis of Polymerization Data. Lag time, V_{max}, and final turbidity were determined as described (*29*). The lag time was measured as the time elapsed until an increase in turbidity was seen, V_{max} was measured as the slope at the steepest part of the polymerization curve, and the final absorbance at 350 nm was read at 40 min for the batroxobin experiments and at 60 min for the thrombin experiments. Statistical values comparing normal and variant recombinant fibrinogens were determined using unpaired *t*-tests. A difference was considered significant when the *p* value was <0.05.

Preparation and Crystallization of D Fragment from BβD398A Fibrinogen. Fragment D of variant BβD398A (rfD-BβD398A) was generated by methods mirroring those for normal fibrinogen fragment D (*9*). Crystals of rfD-BβD398A were grown at 4 °C by sitting-drop vapor diffusion, and initial screening conditions were similar to those previously reported (*5*, *7*−*9*, *30*). The crystals of rfD-BβD398A were grown from drops made by mixing 5 μL of 12 mg/mL protein in 50 mM Tris, pH 7.4, with an equal volume of well solution. The sitting drop was equilibrated by vapor diffusion against the well solution. The well solution contained 50 mM Tris, pH 8.5, 70 mM $CaCl_2$, 2 mM NaN_3, and 14−15% PEG 3350 (wt/vol). Streak seeding from crystals of normal rfD was performed to maximize the growth of diffraction-quality crystals. Crystals grew as clustered plates in a period of days. Single crystals for X-ray diffraction were obtained by carefully separating single crystals from the large clusters with a crystal loop.

Recombinant fragment D of BβD398A was cocrystallized with GHRPam (rfD-BβD398A+GH) in sitting drops at 4 °C prepared by mixing 5 μL of protein solution, composed of 10 mg/mL of rfD-BβD398A in 50 mM Tris, pH 7.4, and 4 mM GHRPam with 5 μL of well solution containing 50 mM Tris, pH 8.5, 2 mM NaN_3, 12.5 mM $CaCl_2$, and 9%

Table 1: X-ray Crystallography Data and Refinement Statistics

	rfD-BβD398A	rfD-BβD398A+GH
resolution (Å)	18−2.7	18−2.45
space group	$P2_12_12_1$	$P2_12_12_1$
cell constants (Å)	$a = 88.5$	$a = 54.5$
	$b = 94.5$	$b = 147.7$
	$c = 227.1$	$c = 229.7$
molecules/asymmetric unit	2	2
total observations	258983	440938
unique reflections	47513	68081
mean redundancy	5.5	6.5
R_{sym}[a] (%; highest shell)	11.1 (48.2)	10.5 (55.5)
completeness (%; highest shell)	89.0 (91.3)	98.5 (91.4)
mean I/σ (highest shell)	8.8 (1.8)	17.5 (2.3)
R_{cryst}[b] (%)	22.0	22.2
R_{free}[c] (%)	27.1	26.3
RMSD bond lengths (Å)	0.0066	0.0065
RMSD bond angles (deg)	1.22	1.28
average *B*-factor	41.9	40.1
number of model atoms	10761	10799
number solvent sites	164	244

[a] $R_{sym} = \sum|I - \langle I\rangle|$ where I is the observed intensity and $\langle I\rangle$ is the average intensity of multiple symmetry-related observations of that reflection. [b] $R_{cryst} = \sum||F_{obs}| - |F_{calc}||/\sum|F_{obs}|$, where F_{obs} and F_{calc} are the observed and calculated structure factors, respectively. [c] $R_{free} = \sum||F_{obs}| - |F_{calc}||/\sum|F_{obs}|$ for 5% of the data withheld from structural refinement.

PEG 3350. Crystals appeared in days, following streak seeding with crystals of normal rfD.

X-ray Diffraction Data Collection. Data collection for rfD-BβD398A+GH was carried out at 100 K with a Rigaku RUH3R rotating anode generator with Osmic confocal blue multilayer optics and Rigaku R-AXIS IV^{2+} detector at the University of North Carolina at Chapel Hill. Due to the small size of rfD-BβD398A crystals, data were collected at 100 K at the SER-CAT beamline 22-ID of Advanced Photon Source. Crystals were prepared for low-temperature data collection by cryoprotecting in a solution that contained 20% glycerol in addition to the crystallant. The cryprotected crystals in loops were flash frozen in liquid nitrogen and stored under liquid nitrogen. X-ray diffraction data sets were processed using DENZO and SCALEPACK (*31*).

Structure Determination. Because the unit cell dimensions for rfD-BβD398A (Table 1) were isomorphous to those reported for normal rfD (*9*), the structure of rfD-BβD398A was refined by rigid body minimization followed by simulated annealing using the rfD structure (PDB code = 1LT9) as a starting model. The refinement was carried out using the program CNS (*32*) and the aspartate at position Bβ398 in the starting model was substituted with an alanine. The structure of rfD-BβD398A+GH was solved by molecular replacement using AMoRe (*33*). The rotation search was carried out using one molecule of the structure of plasma D fragment with GHRPam bound (1FZG) in the resolution range of 8.0−4.0 Å. Two separate solutions were found with correlation coefficients of 72.7 and *R*-factors of 36.7 after rigid-body fitting.

Least-squares minimization, simulated annealing, and individual temperature factor refinement including the use of an overall anisotropic *B*-factor and a bulk solvent correction were used during refinement in CNS (*32*). Before refinement, 5% of the observed data was reserved for cross-validation using the free *R*-factor statistic (*34*). After one round of refinement in CNS, manual rebuilding was done in the program O (*35*) utilizing σA-weighted $|2F_o - F_c|$ and $|F_o - F_c|$ electron density maps (*36*) to guide fitting. The models were improved by cycles of refinement and manual fitting, using the working *R*-factor and free *R*-factor to guide progress. In the final stages of refinement, 164 and 244 solvent molecules were added to the structures of rfD-BβD398A and rfD-BβD398A+GH, respectively. In addition, cis peptide bonds were added at positions Bβ407 and γ339. In the rfD-BβD398A structure before the addition of water molecules and the appropriate cis peptide bonds the *R*-factor and free *R*-factor were 23.7% and 28.7%, respectively, while after these additions the *R*-factor and free *R*-factor dropped to 22.0% and 27.1%, respectively. In the rfD-BβD398A+GH structure, the same revisions resulted in the *R*-factor and free *R*-factor being reduced from 24.6% and 28.7%, respectively, to 22.2% and 26.3%, respectively.

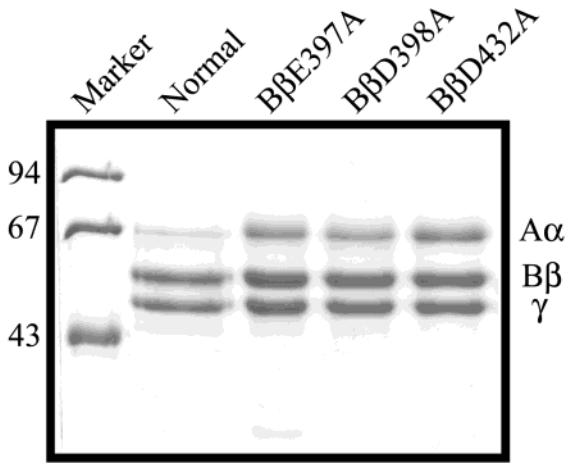

FIGURE 1: SDS−PAGE gel of the recombinant fibrinogens. Reduced samples of normal, BβE397A, BβD398A, and BβD432A fibrinogens were run on a 10% gel. The position of the individual polypeptide chains is indicated (right). The molecular mass markers labeled (left) are in kDa.

RESULTS

Characterization of Recombinant Fibrinogens. We synthesized three variant fibrinogens with single amino acid substitutions in the C-terminal region of the Bβ-chain: Glu397 to Ala (BβE397A), Asp398 to Ala (BβD398A) and Asp432 to Ala (BβD432A). The expression vectors were made by oligonucleotide mutagenesis and transfected into CHO-cell lines, and the clones that produced the highest fibrinogen level for each variant were used for large-scale production, as described in Materials and Methods. The purity and proper polypeptide chain composition of the three synthesized variant fibrinogens were analyzed with SDS−PAGE (Figure 1).

The concentration of secreted fibrinogen varied considerably; the pooled medium from the variants BβD398A and BβD432A contained 2−4 μg/mL fibrinogen, while the pooled medium from BβE397A line contained only 0.4−0.7 μg/mL. We repeated the transfection and selection procedure for variant BβE397A but were not able to identify a cell line with a higher level of secretion. Antifibrinogen western blot assays of cell lysate showed that the low yield of BβE397A was likely due to insufficient synthesis and not to impaired secretion of fibrinogen (data not shown). Because we could purify only small amounts of BβE397A fibrinogen,

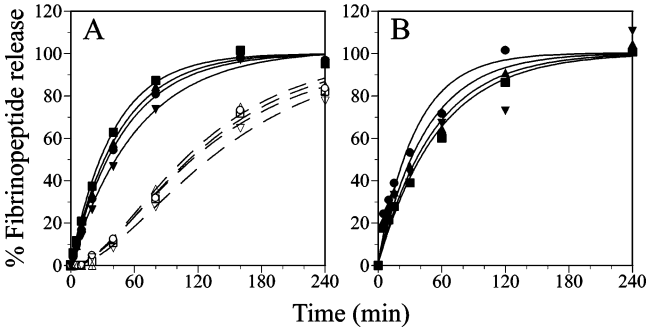

FIGURE 2: Kinetics of FpA and FpB release. Panel A shows thrombin-catalyzed release of FpA (filled symbols) and FpB (open symbols) of normal (■,□), BβD398A (●,○), BβE397A (▲,△), and BβD432A (▼,▽) fibrinogen. Panel B shows batroxobin-catalyzed release of FpA (solid symbols) of normal (■), BβD398A (●), BβE397A (▲), and BβD432A (▼) fibrinogen. FpB was not detected in the reactions with batroxobin. Reactions were initiated by adding 0.005 U/mL thrombin or batroxobin to 0.1 mg/mL fibrinogen as outlined in the Materials and Methods.

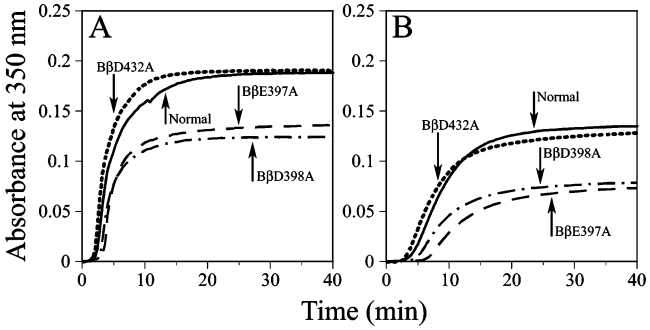

FIGURE 3: Representative polymerization curves for normal (—), BβD398A (— · —), BβE397A (— — —), and BβD432A (···) fibrinogens with thrombin (panel A) and batroxobin (panel B). Conditions for the reactions in panel A were ambient temperature, 0.2 mg/mL fibrinogen, 0.1 U/mL thrombin, and 1 mM $CaCl_2$. Conditions for batroxobin polymerization were ambient temperature, 0.1 mg/mL fibrinogen, 0.1 U/mL batroxobin, and 1 mM $CaCl_2$. Curves shown are of averaged data.

we were not able to prepare BβE397A fragment D for crystallization.

Thrombin- or Batroxobin-Catalyzed Fibrinopeptide Release. Thrombin-catalyzed release of FpA and FpB and batroxobin-catalyzed release of FpA were measured as peak areas following separation by HPLC. FpB was not detected in any reaction with batroxobin (data not shown). As shown in Figure 2, release of FpA and FpB by thrombin (Figure 2A) and release of FpA by batroxobin (Figure 2B) from all three variants was not significantly different from fibrinopeptide release from normal fibrinogen. These data show that the rate of fibrin monomer generation was similar for the variants and for normal fibrinogen, therefore allowing direct comparison of their polymerization profiles. These results also showed that the mutations in the C-terminal part of the Bβ-chain did not affect the catalytic activity of thrombin or batroxobin and verified that batroxobin cleaved FpA, exclusively.

Thrombin-Catalyzed Polymerization. Polymerization experiments were performed with 0.2 mg/mL fibrinogen and 0.1 U/mL human α-thrombin in a 96-well plate measuring the change of turbidity at 350 nm, as described in Materials and Methods. The reactions were performed at three $CaCl_2$ concentrations—without added calcium, 1 mM, and 10 mM—with the Cl^- concentration held constant to exclude the previously described variation due to chloride concentration (*37*). Representative polymerization curves at 1 mM calcium are shown in Figure 3A; averaged data from all conditions are presented in Table 2. We found a prolonged lag time, a reduced V_{max}, and a reduced final turbidity with the variants BβE397A and BβD398A under all conditions, which is indicative of delayed polymerization and altered final clot structure. In contrast, the variant BβD432A polymerized similarly to, or even slightly more rapidly than, normal fibrinogen under all conditions. Although calcium concentration altered polymerization, as shown in Table 2, the changes seen with each of the variants mimicked, in general, the changes seen with normal fibrinogen.

Batroxobin-Catalyzed Fibrinogen Polymerization. Polymerization experiments were performed with 0.1 mg/mL fibrinogen and 0.1 U/mL batroxobin at two $CaCl_2$ concentrations as described in Materials and Methods. Representative curves at 1 mM calcium are shown in Figure 3B; averaged data from all reactions are listed in Table 3. As with thrombin, batroxobin-catalyzed polymerization data revealed a prolonged lag time, a reduced V_{max}, and a reduced final absorbance only with the variants BβE397A and BβD398A. Polymerization of the variant BβD432A was very similar to polymerization of normal fibrinogen. As in thrombin-catalyzed polymerization experiments, the differences between normal and variant fibrinogens were not reduced or eliminated by changing calcium concentrations. The extent of impaired polymerization of BβE397A and BβD398A with batroxobin was similar to the impairment observed for polymerization with thrombin. These data show that β-chain residues continue to influence polymerization when only the "A" polymerization site is exposed.

Table 2: Thrombin-Catalyzed Polymerization Parameters of Normal, BβE397A, BβD398A, and BβD432A Fibrinogen[a]

	lag time (s)	V_{max} ($\times 10^{-4}$ s^{-1})	final ABS at 350 nm[b]
Normal			
no added $CaCl_2$	167 ± 11	2.6 ± 0.17	0.151 ± 0.011
1 mM $CaCl_2$	144 ± 12	3.0 ± 0.04	0.186 ± 0.039
10 mM $CaCl_2$	173 ± 6	3.3 ± 0.26	0.204 ± 0.018
BβE397A			
no added $CaCl_2$	215 ± 14[c]	1.6 ± 0.17[c]	0.116 ± 0.021[c]
1 mM $CaCl_2$	197 ± 6[c]	2.5 ± 0.4	0.137 ± 0.004
10 mM $CaCl_2$	241 ± 18[c]	2.6 ± 0.25[c]	0.144 ± 0.014[c]
BβD398A			
no added $CaCl_2$	166 ± 13	1.6 ± 0.13[c]	0.116 ± 0.011[c]
1 mM $CaCl_2$	167 ± 3[c]	2.5 ± 0.08[c]	0.126 ± 0.004[c]
10 mM $CaCl_2$	220 ± 5[c]	2.1 ± 0.15[c]	0.140 ± 0.014[c]
BβD432A			
no added $CaCl_2$	130 ± 20	2.7 ± 0.56	0.158 ± 0.004
1 mM $CaCl_2$	115 ± 11[c]	3.7 ± 0.22[c]	0.189 ± 0.014
10 mM $CaCl_2$	161 ± 7	3.8 ± 0.33	0.211 ± 0.018

[a] $n \geq 3$ for each value. [b] Final ABS was determined as the absorbance at 350 nm at the 60 min time point of a thrombin-catalyzed polymerization reaction. [c] Signifies values found to be statistically different when compared to normal fibrinogen by an unpaired *t*-test (p values < 0.05).

Structures of rfD-BβD398A. We were able to solve 2.7 Å and 2.45 Å X-ray crystal structures of rfD-BβD398A and rfD-BβD398A+GH, respectively. In both structures, the substitution of aspartic acid with alanine at position 398 in the β-chain was evident in electron density maps. It is

Table 3: Batroxobin-Catalyzed Polymerization Parameters of Normal, BβE397A, BβD398A, and BβD432A Fibrinogen[a]

	lag time (s)	V_{max} ($\times 10^{-4}$ s^{-1})	final ABS at 350 nm[b]
	Normal		
1 μM $CaCl_2$	361 ± 24	2.1 ± 0.1	0.130 ± 0.009
1 mM $CaCl_2$	240 ± 62	2.8 ± 0.5	0.135 ± 0.005
	BβE397A		
1 μM $CaCl_2$	565 ± 56[c]	0.9 ± 0.1[c]	0.060 ± 0.01[c]
1 mM $CaCl_2$	370 ± 8[c]	1.3 ± 0.1[c]	0.074 ± 0.008[c]
	BβD398A		
1 μM $CaCl_2$	423 ± 38	1.2 ± 0.1[c]	0.073 ± 0.004[c]
1 mM $CaCl_2$	279 ± 44	1.7 ± 0.1[c]	0.079 ± 0.008[c]
	BβD432A		
1 μM $CaCl_2$	308 ± 51	2.1 ± 0.4	0.133 ± 0.008
1 mM $CaCl_2$	183 ± 47	3.0 ± 0.3	0.128 ± 0.008

[a] $n \geq 3$ for each value. [b] Final ABS was determined as the absorbance at 350 nm at the 40 min time point of a batroxobin-catalyzed polymerization reaction. [c] Signifies values found to be statistically different when compared to normal fibrinogen by an unpaired *t*-test (*p* values < 0.05).

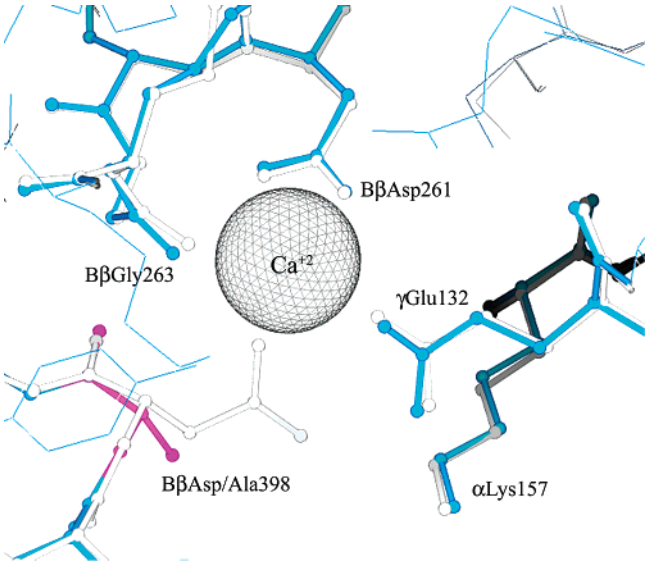

FIGURE 4: Comparison of the β2 calcium-binding site in rfD-BβD398A versus normal rfD (1LT9). The structure represented in gray is rfD, while the structure represented in blue is rfD-BβD398A. The purple residue is the alanine substituted residue at position Bβ398 in the rfD-BβD398A structure. A sphere represents the position of the calcium atom for both structures. The structures show remarkable overlap, indicating little change in the variant compared to normal. It must be noted that the calcium atom modeled in the β2-site of the rfD-BβD398A structure is only 50% occupied whereas in the rfD structure it is 100% occupied.

important to note that the global structure of rfD-BβD398A was not changed by this substitution. In fact, the alignment of rfD-BβD398A with normal rfD results in an RMSD of 0.53 Å over all atoms, showing that the structures are in excellent agreement. Figure 4 shows the remarkable structural similarity of rfD-BβD398A and rfD in the vicinity of the mutation. The primary differences in the variant structures when compared to normal rfD structures were apparent only in specific local interactions that were altered by the alanine substitution.

Peptide Binding in Crystal Structures. We synthesized the variant BβD398A to disrupt the "B:b" interaction and gain insight into role of "B:b" in polymerization. As previously reported, a comparison of normal fragment D structures in the absence and presence of the "B" peptide, GHRPam, showed that BβGlu397 and BβAsp398 are repositioned upon peptide binding (*8*, *9*). In the absence of peptide, BβAsp398 coordinates calcium in the β2-site; upon binding of peptide at the "b" polymerization site, BβAsp398, along with BβGlu397, flips 180° to interact with the arginine side chain of GHRPam. Variant crystals were grown in the presence of 4 mM GHRPam, which is a 40× molar excess over protein concentration. The structure of rfD-BβD398A+GH showed peptide was not present in the "b" site, Figure 5A. No difference electron density corresponding to the peptide was found, Figure 5A, in contrast with corresponding difference electron density of the peptide bound to the "b" site in normal rfD (1LTJ), Figure 5B. Indeed, neither BβGlu397 nor the altered residue BβAla398 flipped toward the "b" site, so these residues were not seen in Figure 5A. Rather these residues remained in their original positions, such that a comparison of the β-chain residues 261−263 and 397−399 in rfD-BβD398A+GH and rfD-BβD398A gave an overall root-mean-square deviation (RMSD) of only 0.54 Å. These data confirmed that the substitution of alanine at residue Bβ398 eliminated the "B:b" interaction and the associated changes in the positions of residues Bβ397 and Bβ398.

As has been seen with plasma fibrinogen fragment D (*8*), the structure of rfD-BβD398A+GH showed the peptide GHRPam bound in the "a" polymerization site of the variant fibrinogen. GHRPam was bound to the "a" site of both molecules in the asymmetric unit of our crystal, although, as shown in Figure 6, the conformation of the peptide in one molecule differed from that in the second. In one molecule of the asymmetric unit, Figure 6A, the conformation of the peptide resembled the structure of GHRPam bound to the "b" polymerization site of normal fibrinogen (Figure 6C), while in the second molecule of the asymmetric unit (Figure 6B), the histidine side chain pointed in the opposite direction. Figure 6D shows an alignment of these three conformations to demonstrate the movement of the histidine side chain of bound GHRPam. As described in the following paragraphs, the γ2 calcium-binding site, which appeared concomitant with GHRPam binding to the "a" site, was also asymmetric in the rfD-BβD398A+GH structure. When GHRPam was bound to the "a" site in the conformation that resembled the structure in the "b" site, calcium was not present (Figure 6A), while in the alternate conformation (Figure 6B) calcium was present at the γ2-site. We attribute these differences in structure to the unique constraints of crystal packing interactions occurring with each of the two molecules in the asymmetric unit.

Calcium Binding in Crystal Structures. X-ray crystal structure data of rfD-BβD398A and rfD-BβD398A+GH showed impaired calcium binding at the β2-site. As previously mentioned, the β2-site is located adjacent to the "b" polymerization site and is comprised of the side chain carbonyls of residues BβAsp398, BβAsp261, and γGlu132 and the backbone carbonyl oxygen of residue BβGly263. Thus, the substitution of alanine for aspartic acid Bβ398 eliminated one coordinating oxygen in the β2-site. The electron density for the rfD-BβD398A structure, determined from crystals grown at 70 mM $CaCl_2$, showed the β2-site was reduced to 50% occupancy. The reduced occupancy in

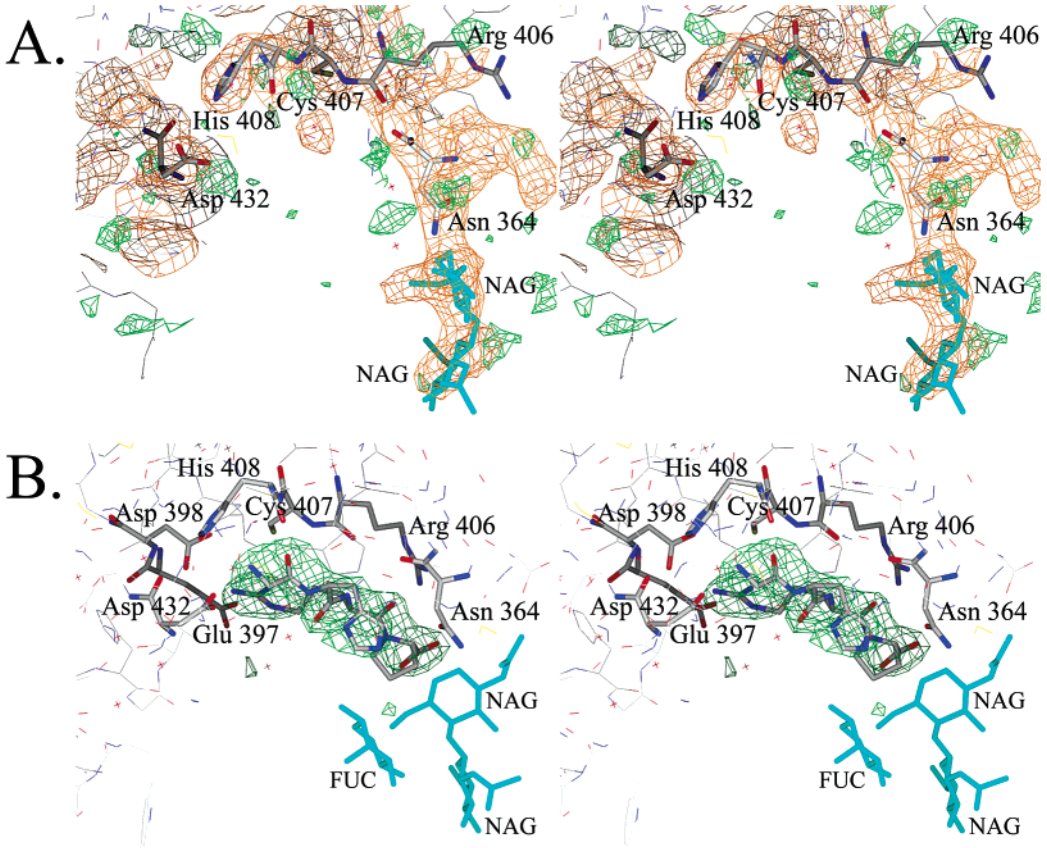

FIGURE 5: Stereodiagrams of the "b" polymerization site in rfD-BβD398A+GH (panel A) and rfD-BOTH (1LTJ, panel B). Difference electron density ($|F_o - F_c|$) is contoured at 3.0σ and is shown in both panels A and B in shades of green. In panel A, $|2F_o - F_c|$ electron density at 1.0σ is shown in shades of orange-brown for residues lining the "b" site. Residues lining the pocket are labeled in each panel. Carbohydrate is shown in light blue. Notice that strong difference electron density is seen in panel B for the presence of GHRPam in the "b" site in rfD-BOTH, but strong difference density is not seen in variant structure in panel A, meaning that no peptide is present. In addition, note that residues Bβ398 and Bβ397 are present in panel B and not in panel A, consistent with the lack of peptide in the "b" polymerization site of rfD-BβD398A+GH (panel A).

the face of 35 times the physiologic calcium concentration indicates that coordination by BβAsp398 is critical for calcium binding at the β2-site. In fact, the rfD-BβD398A+GH structure, obtained with crystals grown at much lower calcium, 12.5 mM, showed insufficient density for any calcium at this site. Moreover, as shown in Figure 7, the side chain carbonyl of a second coordinating residue, γGlu132, has formed a new salt link with residue αLys157. These data indicate that calcium will not be bound at the β2-site in BβD398A fibrinogen at the calcium ion concentrations used for our polymerization experiments.

The rfD-BβD398A+GH structure also showed calcium bound to the γ2-site (Figure 6B), which is composed of the side chains of residue γAsp294 and γAsp301 and the backbone carbonyls of γGly296 and γAsp298. As described above, calcium has been observed in the γ2-site only when GHRPam is bound in the "a" site. Our data are consistent in this regard, with previous observations with plasma fragment D and double D fragment crystals in the presence of GHRPam (*8*). It must be noted, however, that in our rfD-BβD398A+GH structure the calcium atom was present in the γ2-site in only one of the two molecules in the asymmetric unit.

DISCUSSION

This study examined three engineered variant fibrinogens with alanine substitutions at residues BβGlu397, BβAsp398, and BβAsp432. These changes targeted residues that appeared to participate in the "B:b" interaction as shown in several crystallographic structures (*7*, *8*). Our goal was 2-fold: to identify residues that are critical for the "B:b" interaction and to determine the impact of the "B:b" interaction on polymerization. When considered together, our experimental results support the following conclusions: (1) residues BβGlu397 and BβAsp398 are essential to establishing the "B:b" interaction, while residue BβAsp432 is not; (2) the residue BβAsp398 is necessary for calcium-binding at the β2-site when calcium concentration is $\leq$12.5 mM; (3) the "A:b" interaction is a part of normal batroxobin polymerization.

Thrombin-catalyzed polymerization experiments performed at several calcium concentrations showed an increased lag time, reduced V_{max}, and lower final turbidity for BβE397A and BβD398A when compared to normal fibrinogen. The reduced rate of protofibril formation and lateral aggregation of protofibrils demonstrates that BβGlu397 and BβAsp398 are important for normal fibrin clot formation. The 2.45 Å crystal structure of rfD-BβD398A+GH confirmed that BβAsp398 is essential for the "B:b" interaction, as the peptide, GHRPam, was not bound in the "b" polymerization site even when the crystals were grown in the presence of a 40$\times$ molar excess of peptide. As expected, the conformational change of residues Bβ397 and Bβ398, which take place when GHRPam binds to the normal "b"

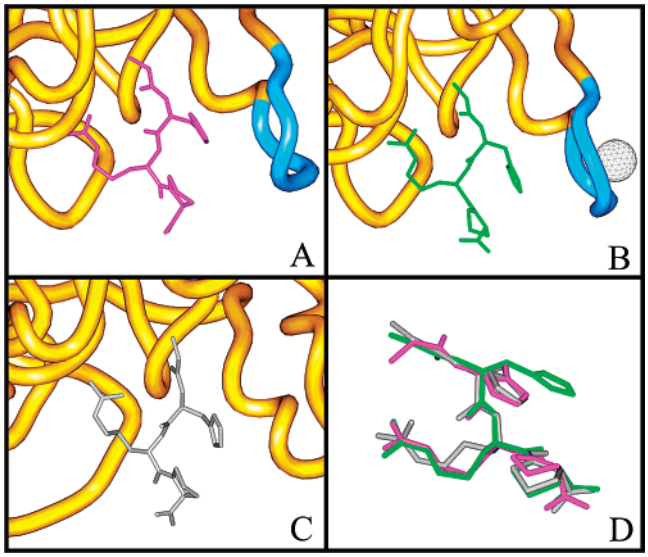

FIGURE 6: Comparison of observed GHRPam conformations. Panel A shows the conformation of GHRPam (purple) bound in the "a" polymerization site of one molecule of the asymmetric unit of the rfD-BβD398A+GH crystal. Panel B shows the conformation of GHRPam (green) in the "a" polymerization site of the second molecule in the asymmetric unit of the rfD-BβD398A+GH crystal along with a calcium atom (sphere) bound in the γ2-site (blue). Notice that no calcium is bound in panel A and the peptide's conformation in panel A is different than the conformation in panel B. Panel C depicts GHRPam (gray) bound in the "b" polymerization site. Note that the conformation of GHRPam in panels A and C is similar. Panel D shows the GHRPam conformations aligned by Cα backbone, to clearly illustrate the different positions of the histidine side chain between the conformation in panel B and those in panels A and C.

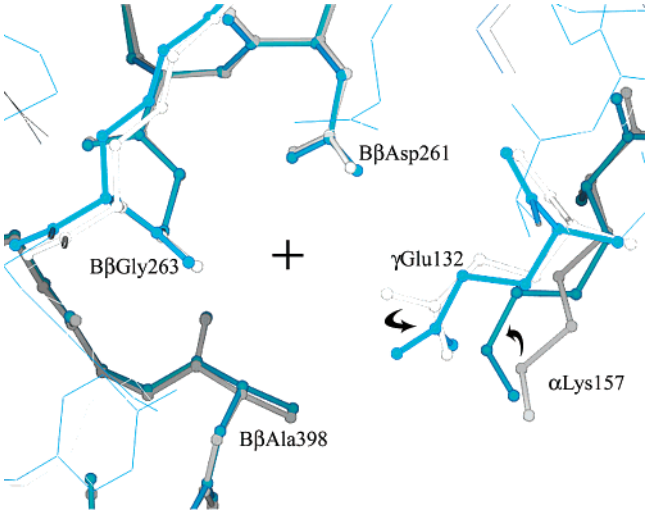

FIGURE 7: Comparison of the β2 calcium-binding site structure in the crystal of rfD-BβD398A (shades of gray) and rfD-BβD398A+GH (shades of blue). The calcium atom's position in the rfD-BβD398A structure is represented as a black cross, while there is no calcium atom present in the rfD-BβD398A+GH structure (blue). Notice the overlap between structures except for the residues γGlu132 and αLys157. Residue γGlu132 participates in coordinating calcium in the rfD-BβD398A structure, while in the rfD-BβD398A+GH structure it moves away from that coordinating position to form a salt link with residue αLys157 (indicated by arrows).

polymerization site, did not occur. These data clearly present the case for the loss of the "B:b" interaction in the variant BβD398A, and we conclude that this loss led to the impaired polymerization of this variant. Because polymerization of BβE397A was similarly or even more impaired, we infer that BβGlu397 is also essential to a normal "B:b" interaction. It is unfortunate that low protein production hindered our ability to crystallize the BβE397A variant.

Batroxobin-catalyzed polymerization profiles for variants BβE397A and BβD398A when compared to normal recombinant fibrinogen were impaired similarly to thrombin-catalyzed polymerization. Initially, we expected to see no difference in batroxobin-catalyzed polymerization of normal and variant fibrinogens. We formed this hypothesis because batroxobin cleaves FpA only and therefore we inferred that polymerization would only be driven by "A:a" interactions. The "B:b" interactions, which are not possible in BβE397A and BβD398A variants, would be irrelevant during batroxobin-catalyzed polymerization. Our expectations were incorrect. Batroxobin-catalyzed polymerization of BβE397A and BβD398A variants was impaired. Although we lack direct evidence for the "A:b" interaction in fibrin, the batroxobin experimental results suggest that in addition to "A:a" interactions "A:b" interactions participate in batroxobin-catalyzed polymerization. By inference, these data also suggest that "A:b" interactions are a part of normal thrombin-catalyzed fibrin polymerization. That is, the lack of "A:b" interactions due to an impaired "b" site in BβE397A and BβD398A fibrinogens is responsible for the differences seen in batroxobin-catalyzed polymerization of BβE397A and BβD398A fibrinogens compared to normal fibrinogen. The possibility of "A:b" interactions has been proposed previously to explain the finding that GPRPam can bind to four sites in one fibrinogen molecule (*38*). We have also seen the existence of "A:b" interactions in some of our recombinant fibrinogen fragment D structures, in which GPRPam is bound to the "b" polymerization site (manuscript in preparation).

In contrast to BβE397A and BβD398A fibrinogens, thrombin- and batroxobin-catalyzed polymerization of the BβD432A variant was essentially normal, suggesting that BβAsp432 is not critical to the function of the "b" polymerization site. We were surprised by this result because crystallographic structures of plasma fibrinogen fragments D and D−D in the presence of GHRPam suggested that BβAsp432 is a key residue for the "B:b" interaction, forming an ionic interaction between the negatively charged side chain carbonyl and the positively charged amino terminus of the peptide (*7*, *8*). Moreover, substitutions at two residues in the "a" polymerization site that interact analogously with the charged amino terminus of the peptide GPRPam, γAsp330 and γAsp364, have profound effects on polymerization (*23*, *39*−*42*). Two different substitutions at residue γAsp330, D330V and D330Y, have been identified in people, the former in both homozygous and heterozygous individuals (fibrinogens Ales, Milano I, and Kyoto III) (*39*−*41*). Polymerization of fibrinogen isolated from these individuals was impaired, as expected if critical "A:a" interactions were compromised. Fibrinogens with substitutions at residue γAsp364 have been identified in people and synthesized by recombinant techniques (fibrinogens Matsumoto I and Melun I) (*23*, *42*). Again, in all cases polymerization was markedly impaired. We therefore expected that changing the charged aspartate residue to alanine would weaken the "B:b" interaction. Taking into account the structural homology of the "a" and "b" polymerization sites, it is puzzling that the changes

in the "a" site variants do impact polymerization while the analogous mutation in the "b" site does not. Perhaps this difference reflects the number of interactions that support "B:b" relative to "A:a" or that BβAsp432 is simply less critical to "B:b" than either γAsp330 or γAsp364 is to "A:a". Alternatively, it is possible that a compensating conformational change has occurred in variant BβD432A, such that new interactions would be relevant to GHRPam binding. We chose not to crystallize this variant because its polymerization was normal; therefore, our data are not sufficient to distinguish among these possibilities.

Analysis of the structures presented in Figure 4 revealed that the structure of variant BβD398A in the region of the substitution is essentially the same as the structure of normal recombinant fibrinogen except that the β2 calcium-binding site was reduced to approximately 50% occupancy. The reduced calcium binding was anticipated from the loss of the carboxylate side chain of BβAsp398, which serves as a calcium ligand. In fact, when crystals were grown under conditions of lower calcium concentration, 12.5 mM, which allowed crystal formation in the presence of peptide GHRPam, this calcium-binding site was entirely unoccupied. Under these crystallization conditions with recombinant fragment D of BβD398A fibrinogen, neither calcium nor GHRPam was bound to the β2-site or "b" polymerization site, respectively. In addition, residues Bβ398 and Bβ397 remained in the positions corresponding to the positions seen in normal rfD with no peptide ligands bound (1LT9) (*9*). In agreement with data from normal rfD, the loss of calcium from the β2-site in the rfD-BβD398A+GH structure is associated with the formation of a new salt link between the side chains of residues γGlu132 and αLys157 (*9*). This conformational change is analogous to the one seen with normal rfD in the presence of GHRPam (1LTJ) in that BβAsp398 binds GHRPam, calcium is absent in the β2-site. and the salt link between γGlu132 and αLys157 is present (*9*). Considered together, these results suggest that at 12.5 mM calcium concentration, the loss of the BβAsp398 carboxylate, either through alternate interactions with bound peptide or through substitution to alanine, leads to the loss of calcium binding and to the formation of the salt link between γGlu132 and αLys157. This conformational change removes the calcium anchor between the globular module of the Bβ-chain and the coiled-coil, opening the possibility for the β-module to move relative to the other parts of the fibrin molecule (*9*).

The structural data imply that calcium will not be bound at the β2-site in variant fibrinogen BβD398A under any of the conditions that we have used in our polymerization experiments, while by inference calcium should be bound at the β2-site in BβE397A fibrinogen, because residue Bβ397 is not a calcium-coordinating residue of the β2-site (*9*). At the same time, the data from polymerization experiments performed at different calcium concentrations suggest that calcium affects BβD398A and BβE397A fibrinogens in a similar way. That is, the differences in polymerization seen when comparing BβD398A and BβE397A to normal fibrinogen largely arise from the loss of normal "B:b" interactions rather than the loss of calcium binding at the β2-site. The implication of this is that the loss or impairment of "B:b" interactions has a greater effect on polymerization than the loss of the calcium anchor. In contrast, when the β2-site is lost in another variant synthesized in our laboratory, γE132A, that preserved "B:b" interactions, we found that polymerization was markedly dependent on calcium in an unusual manner relative to normal fibrinogen (see our second paper in this issue). Thus, we do not conclude that the β2-site is insignificant in controlling polymerization.

In resolving the crystal structure of rfD-BβD398A+GH, we were surprised to see two conformations of GHRPam bound in the "a" site. One conformation resembled GHRPam bound to the "b" site, while the other was a novel conformation with a shifted histidine side chain and appeared in conjunction with calcium binding in the γ2-site. Since this novel conformation was seen in only one of the two molecules in the asymmetric unit, it is likely that both the altered conformation and calcium binding in the γ2-site were induced by crystal packing constraints. Data supporting this conclusion were seen in the crystal structure of rfD-γE132A in the presence of GHRPam (see our second paper in this issue). These two conformations of GHRPam peptide bound to the "a" site reveal an intrinsic flexibility of both the "a" and "B" polymerization sites. Such flexibility probably accounts for the variety of crystal forms for fragment D and may be relevant to the molecular interactions that mediate polymerization.

In summary, we have produced and studied three variant fibrinogens with alanine substitutions in the "b" polymerization site with goals of defining critical residues in mediating the "B:b" interaction and determining the impact of "B:b" interactions on polymerization. We determined that two residues, BβD398 and BβE397, are necessary to support the binding of GHRPam to the "b" polymerization site, while residue BβD432 is not. Variants BβD398A and BβE397A reveal that residues BβD398 and BβE397 are involved in both protofibril formation and lateral aggregation. In addition, our structural data with variant BβD398A support previous data showing that residue BβD398 is critical to controlling calcium binding to the β2-site. Furthermore, experiments with batroxobin suggested that the "A:b" interactions are a normal part of batroxobin polymerization. Finally our structure data showed that the γ2 calcium-binding site was asymmetric in our crystal of rfD-BβD398A+GH suggesting that this site is a consequence of crystal packing interactions and not of GHRPam binding to the "a" site.

ACKNOWLEDGMENT

We thank Dr. Matthew R. Redinbo (UNC-CH, Chapel Hill, NC) for his guidance throughout this project and Dr. Brenda Temple at the UNC-CH Structural BioInformatics Core Facility (Chapel Hill, NC) for use of the computing facilities. We thank Dr. Betsy Merenbloom for reviewing our manuscript, Li Fang Ping for her technical assistance, the National Cell Culture Center for producing culture medium for normal fibrinogen, and the Southeast Regional Collaborative Access Team at Advanced Photon Source for synchrotron time.

NOTE ADDED AFTER ASAP POSTING

This article was released ASAP on 2/10/2004. Subsequently, a change was made to ref 35, and the article was reposted on 2/12/2004.

REFERENCES

1. Hall, C. E., and Slayter, H. S. (1959) *J. Biophys. Biochem. Cytol. 5*, 11−17.
2. Fowler, W. E., and Erickson, H. P. (1979) *J. Mol. Biol. 134*, 241−249.
3. Doolittle, R. F., Goldbaum, D. M., and Doolittle, L. R. (1978) *J. Mol. Biol. 120*, 311−325.
4. Veklich, Y. I., Gorkun, O. V., Medved, L. V., Nieuwenhuizen, W., and Weisel, J. W. (1993) *J. Biol. Chem. 268*, 13577−13585.
5. Spraggon, G., Everse, S. J., and Doolittle, R. F. (1997) *Nature 389*, 455−462.
6. Yee, V. C., Pratt, K. P., Cote, H. C., Trong, I. L., Chung, D. W., Davie, E. W., Stenkamp, R. E., and Teller, D. C. (1997) *Structure 5*, 125−138.
7. Everse, S. J., Spraggon, G., Veerapandian, L., Riley, M., and Doolittle, R. F. (1998) *Biochemistry 37*, 8637−8642.
8. Everse, S. J., Spraggon, G., Veerapandian, L., and Doolittle, R. F. (1999) *Biochemistry 38*, 2941−2946.
9. Kostelansky, M. S., Betts, L., Gorkun, O. V., and Lord, S. T. (2002) *Biochemistry 41*, 12124−12132.
10. Laudano, A. P., and Doolittle, R. F. (1978) *Proc. Natl. Acad. Sci. U.S.A. 75*, 3085−3089.
11. Olexa, S. A., and Budzynski, A. Z. (1980) *Proc. Natl. Acad. Sci. U.S.A. 77*, 1374−1378.
12. Hantgan, R. R., and Hermans, J. (1979) *J. Biol. Chem. 254*, 11272−11281.
13. Laurent, T. C., and Blomback, B. (1958) *Acta Chem. Scand. 12*, 1875−1877.
14. Blomback, B., Hessel, B., Hogg, D., and Therkildsen, L. (1978) *Nature 275*, 501−505.
15. Weisel, J. W. (1986) *Biophys. J. 50*, 1079−1093.
16. Brummel, K. E., Butenas, S., and Mann, K. G. (1999) *J. Biol. Chem. 274*, 22862−22870.
17. Lounes, K. C., Ping, L., Gorkun, O. V., and Lord, S. T. (2002) *Biochemistry 41*, 5291−5299.
18. Pratt, K. P., Cote, H. C. F., Chung, D. W., Stenkamp, R. E., and Davie, E. W. (1997) *Proc. Natl. Acad. Sci. U.S.A. 94*, 7176−7181.
19. Laudano, A. P., and Doolittle, R. F. (1980) *Biochemistry 19*, 1013−1019.
20. Matsuda, M., and Sugo, T. (2001) *Ann. N. Y. Acad. Sci. 936*, 65−88.
21. Weisel, J. W., Veklich, Y., and Gorkun, O. (1993) *J. Mol. Biol. 232*, 285−297.
22. Lord, S. T., Strickland, E., and Jayjock, E. (1996) *Biochemistry 35*, 2342−2348.
23. Okumura, N., Gorkun, O. V., and Lord, S. T. (1997) *J. Biol. Chem. 272*, 29596−29601.
24. Binnie, C. G., Hettasch, J. M., Strickland, E., and Lord, S. T. (1993) *Biochemistry 32*, 107−113.
25. Gorkun, O. V., Veklich, Y. I., Weisel, J. W., and Lord, S. T. (1997) *Blood 89*, 4407−4414.
26. Mihalyi, E. (1968) *Biochemistry 7*, 208−223.
27. Ng, A. S., Lewis, S. D., and Shafer, J. A. (1993) *Methods Enzymol. 222*, 341−358.
28. Mullin, J. L., Gorkun, O. V., and Lord, S. T. (2000) *Biochemistry 39*, 9843−9849.
29. Furlan, M., Rupp, C., and Beck, E. A. (1983) *Biochim. Biophys. Acta 742*, 25−32.
30. Everse, S. J., Pelletier, H., and Doolittle, R. F. (1995) *Protein Sci. 4*, 1013−1016.
31. Otwinowski, Z. M. W. (1997) *Methods Enzymol. 276*, 307−326.
32. Brunger, A. T., Adams, P. D., Clore, G. M., DeLano, W. L., Gros, P., Grosse-Kunstleve, R. W., Jiang, J. S., Kuszewski, J., Nilges, M., Pannu, N. S., Read, R. J., Rice, L. M., Simonson, T., and Warren, G. L. (1998) *Acta Crystallogr., Sect. D 54*, 905−921.
33. Navaza, J. S. P. (1997) *Methods Enzymol. 276*, 581−594.
34. Brunger, A. T. (1993) *Acta Crystallogr., Sect. D 49*, 24−36.
35. Jones, T. A., Zou, J. Y., Cowan, S. W., and Kjeldgaard, M. (1991) *Acta Crystallogr., Sect. A 47*, 110−119.
36. Read, R. J. (1986) *Acta Crystallogr., Sect. A 42*, 140−149.
37. Di Stasio, E., Nagaswami, C., Weisel, J. W., and Di Cera, E. (1998) *Biophys. J. 75*, 1973−1979.
38. Laudano, A. P., Cottrell, B. A., and Doolittle, R. F. (1983) *Ann. N. Y. Acad. Sci. 408*, 315−329.
39. Reber, P., Furlan, M., Rupp, C., Kehl, M., Henschen, A., Mannucci, P. M., and Beck, E. A. (1986) *Blood 67*, 1751−1756.
40. Terukina, S., Yamazumi, K., Okamoto, K., Yamashita, H., Ito, Y., and Matsuda, M. (1989) *Blood 74*, 2681−2687.
41. Lounes, K. C., Soria, C., Mirshahi, S. S., Desvignes, P., Mirshahi, M., Bertrand, O., Bonnet, P., Koopman, J., and Soria, J. (2000) *Blood 96*, 3473−3479.
42. Okumura, N., Furihata, K., Terasawa, F., Nakagoshi, R., Ueno, I., and Katsuyama, T. (1996) *Thromb. Haemostasis 75*, 887−891.

BI035996F